Band gaps in phononic crystals: Generation mechanisms and interaction effects

C. Croënne, E. J. S. Lee, Hefei Hu, and J. H. Page

Citation: AIP Advances **1**, 041401 (2011); doi: 10.1063/1.3675797
View online: http://dx.doi.org/10.1063/1.3675797
View Table of Contents: http://aipadvances.aip.org/resource/1/AAIDBI/v1/i4
Published by the American Institute of Physics.

Band gaps in phononic crystals: Generation mechanisms and interaction effects

C. Croënne,[a] E. J. S. Lee, Hefei Hu,[b] and J. H. Page
Department of Physics and Astronomy, University of Manitoba, Winnipeg, Manitoba R3T 2N2, Canada

(Received 31 October 2011; accepted 9 November 2011; published online 23 December 2011)

A wide range of mesoscopic phononic materials can exhibit frequency bands where transmission is forbidden, i.e. band gaps. Three different mechanisms for their origin can be distinguished, namely Bragg, hybridization and weak elastic coupling effects. Characteristic properties of gaps of different origins are investigated and compared, for a 3D crystal of tungsten carbide beads in water, a 2D crystal of nylon rods in water, and a 3D opal-like structure of weakly sintered aluminum beads. For the second type of crystal, it is shown that Bragg and hybridization gaps can be overlapped, allowing the study of the interaction between these two mechanisms. Atypical dispersion characteristics are demonstrated near the resonance frequency. [doi:10.1063/1.3675797]

I. INTRODUCTION

In the past few years, many studies have been devoted to artificial mesoscopic phononic materials. When the wave phenomena they exhibit depend on the periodic arrangement of scatterers inside the medium, they are usually called phononic crystals (PCs).[1] When they rely on the behavior of the individual inclusions inside the matrix, they are often called metamaterials.[2] In this case, randomly positioned collections of inclusions inside a matrix can be considered, even though, for ease of fabrication and calculation, as well as to readily fix a constant filling factor, periodic arrangements are often used. Additionally, in order to assign effective material parameters to the structures, stringent conditions on the size of the inclusions with respect to the wavelength are generally imposed. In phononic crystals, one of the most usual features is the presence of Bragg gaps, caused by destructive interference of waves scattered from the inclusions.[3,4] As a result, for certain ranges of frequencies, wave propagation may be inhibited in all directions (band gaps) or only along certain directions (stop bands). Interestingly, band gaps with other origins can also be observed in mesoscopic structures. One type is related to the coupling between scattering resonances of the individual inclusions and the propagating mode of the embedding medium,[5–7] which is why they have been called hybridization gaps.[8] In metamaterial systems, such gaps are particularly interesting, since it can be shown that they allow, in some cases, the definition of negative effective material parameters.[9,10] The similarities between the mesoscopic structures which exhibit those two different gap creation mechanisms make it possible to investigate questions raised by their eventual combination. Indeed, it has been demonstrated in previous studies[11] that it was possible to design periodic structures where Bragg and hybridization gaps could be observed in the same frequency region. The combination of Bragg and hybridization effects has also been invoked to explain the remarkably wide bandgaps that have been found both experimentally and theoretically in three dimensional (3D) crystals of dense solid spheres (e.g., steel, tungsten carbide) in a polymeric matrix (e.g., epoxy,

[a]Corresponding author. charles.croenne@gmail.com
[b]Present address: Department of Physics, University of Illinois at Urbana-Champaign, Urbana, Illinois 61801, USA

polyester).[4,12] In[13] and,[14] resonance-related gaps assisted by Bragg effects were demonstrated, based on the study of the displacement fields in one case, and on the evolution of the transmission coefficient as a function of the number of rows in the other case. Finally, a third type of band gap can be observed in systems built from elementary structural units such as solid spheres that are coupled together by elastic bonds. Again, the resonant modes of the individual scatterers are exploited, but the mechanism leading to band gap formation is different: in this case, the weak elastic coupling between resonances creates passbands of limited bandwidth, so that gaps form in between these passbands.

In this paper, we examine these three different mechanisms for band gap formation, leaving aside other interesting properties of the pass bands in PCs, such as negative refraction and focusing.[15–18] In the first section, to illustrate the Bragg effect, a classical 3D crystal of tungsten carbide beads in water is considered.[3,4] Experimental and theoretical transmission spectra in terms of amplitude and phase are shown for two different crystal thicknesses, in order to highlight the characteristic properties of Bragg gaps. In the next section, a nylon/water 2D PC, with successive hybridization and Bragg gaps as a function of frequency is presented, along with the experimental and numerical procedures used in its study. The dispersion characteristics inside the hybridization gap are analyzed, with particular attention given to the group velocity properties. Then, the PC is modified in order to overlap the two gaps, and their interaction is explored by changing the temperature, which modifies the position of the resonance frequency characteristic of the hybridization effect. Atypical dispersion characteristics are found and attributed to the coupling of the resonant states of the individual rods in samples of finite thickness. The interpretation is confirmed by the study of PC slabs with different numbers of rows. In the last section of the paper, a crystal exhibiting the third gap formation mechanism is investigated. This crystal is made of weakly sintered aluminum beads arranged in an opal-like 3D structure, and its transmission properties are compared with those of a sample in which the beads are randomly positioned.

II. CLASSICAL BRAGG EFFECT IN A 3D PC

Bragg effects have been observed for many types of PC structures in the past several years, including crystals with solid or liquid inclusions, in solid or liquid matrices, with different dimensionalities. Here we will take as an example a face-centered-cubic PC made of spherical tungsten carbide beads in water which was the first 3D PC with a large complete band gap to be studied both experimentally and theoretically.[3,4] As shown in Fig. 1, complex transmission spectra were obtained experimentally around the first Bragg gap of the structure, enabling the frequency dependence of the amplitude transmission coefficient and the dispersion relation to be measured. The results were confirmed by calculations using the multiple scattering theory (MST) described in.[19]

The transmission coefficient (Fig. 1(a)) exhibits a wide, smoothly-varying, symmetric dip, centered at 0.945 MHz, which is typical of pure Bragg gaps observed in crystals of finite thickness. As the thickness L of the crystal increases, the transmitted amplitude decreases exponentially in the gap, falling as $\exp[-k''L]$ with k'' ($= 0.93$ mm^{-1} at frequency $f = 0.945$ MHz) characterizing the evanescent decay of the transmitted amplitude and the breakdown of normal wave propagation in the gap. Figure 1(b) shows that this lowest-frequency band gap occurs when the real part of the wave vector reaches the edge of the first Brillouin zone, as expected. The slope of the dispersion curve is very steep and positive in the band gap region, indicating that the group velocity ($d\omega/dk$) is also large and positive, attaining values greater than the velocities of both constituent materials. Insight into the transmission mechanism at band gap frequencies can be obtained by noting that the group velocity v_g increases in proportion to the crystal thickness, an unusual effect that is the classic signature of tunneling in quantum mechanics. This increase in v_g with thickness can be noted from the change of the slopes of the dispersion curves in Fig. 1(b), but was also demonstrated directly in the experiments by measuring the transit time of the peak of narrow-band Gaussian pulses.[3] Thus, both classical wave tunneling through a band gap in phononic crystals and quantum tunneling through a barrier enable a weak signal to be transmitted with a group time that is independent of thickness, unlike normal propagation in which the group velocity is independent of thickness. The group time may be interpreted as a direct measure of the tunneling time in the PC case.

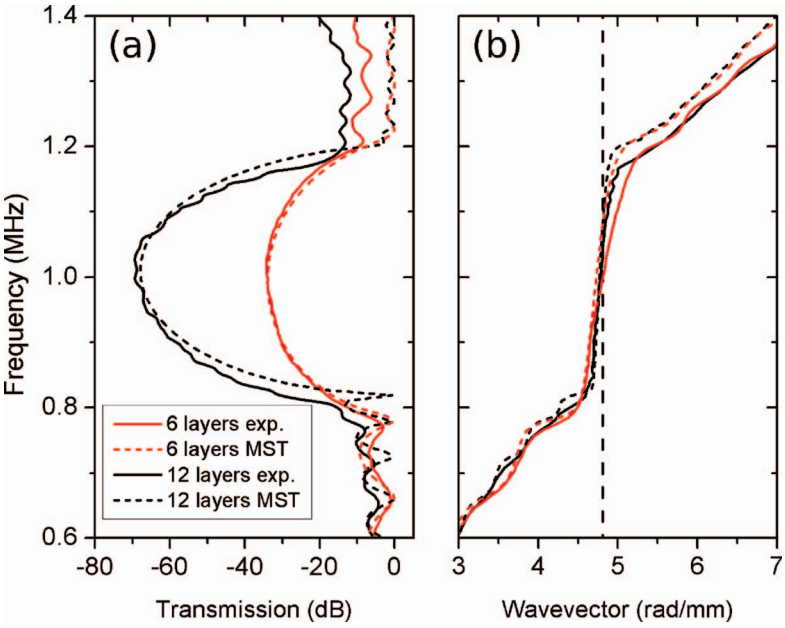

FIG. 1. (Color online) Experimental (solid lines) and numerical (dashed lines, MST method) (a) transmission coefficient and (b) wave vector as a function of frequency, obtained for the six and twelve-layer thick (red and black lines, respectively) 3D PC of tungsten carbide beads in water. The vertical dashed line shows the position of the limit of the first Brillouin zone.

One important difference between classical wave tunneling in phononic crystals and quantum particle tunneling is revealed by examining the phase of the transmitted signals, reflecting the different origins of the gap in the two cases.[3] For quantum tunneling, the real part of the wave vector is zero inside the barrier and the phase difference between input and output sides of the barrier becomes independent of thickness for thick barriers. By contrast, inside the Bragg gap of a PC, due to multiple destructive interference of waves scattered from neighboring inclusions, a standing wave builds up in every layer of the crystal. For the lowest gap, the standing wave wavelength satisfies the Bragg condition that half the wavelength is equal to the thickness of each layer. Propagation ceases because there are no traveling wave solutions. The amplitude of the transmitted field decays evanescently, but the phase difference between pressure fields at the input and output of a cell is a multiple of π and is proportional to the number of layers. Thus the wave vector can be accurately measured and calculated simply by dividing transmission phase by the thickness of the crystal ($k = \phi/L$), and this translates into wave vector values positioned on the boundary of the first Brillouin zone, as shown in Fig. 1(b).

III. PC WITH SUCCESSIVE HYBRIDIZATION AND BRAGG GAPS

In order to highlight the characteristic properties of hybridization gaps, we consider a PC made of a 2D triangular lattice of cylindrical nylon rods in a water matrix. The surrounding medium is also water. Propagation direction is along ΓM, which is the direction normal to the rectangular sample interfaces. Nylon density is $\rho = 1150$ kg/m^3 and longitudinal velocity about 2400 m/s. It can be shown experimentally that shear velocity depends on several parameters, such as temperature, time of immersion in water and vertical tension of the rods. At 25°C, its value is around 950 m/s in our experimental setup.

Experiments are conducted in a water tank with temperature control, using pairs of identical transducers (Panametrics) spanning the frequency range from 0.3 to 2.2 MHz. The measured time signals are Fourier transformed to obtain the frequency dependence of the complex transmission,

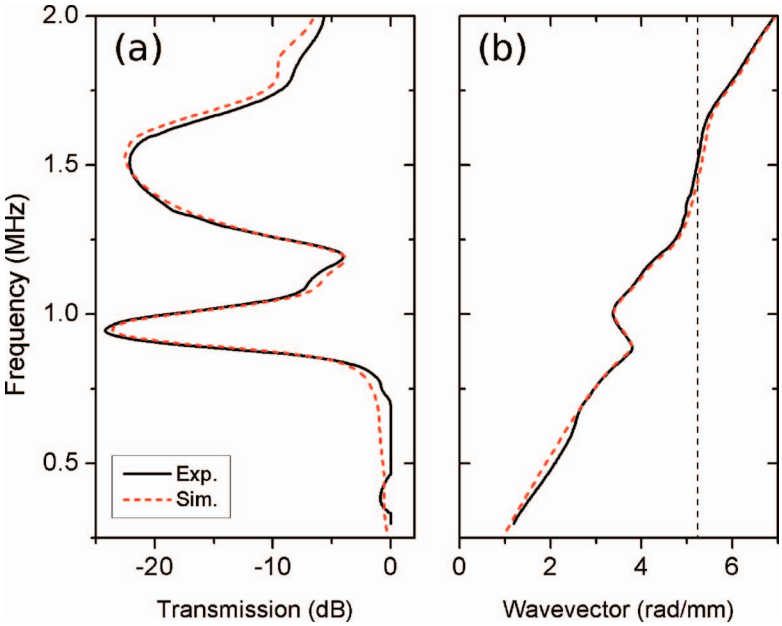

FIG. 2. (Color online) Experimental (solid black lines) and numerical (dashed red lines) (a) transmission coefficient and (b) wave vector as a function of frequency, obtained for the six-layer-thick PC of nylon rods in water with a filling factor of 40%, at 28°C. The vertical dashed line shows the position of the limit of the first Brillouin zone.

so that both amplitude and phase are determined. The PC samples are built from 0.46-mm-diameter nylon rods, readily available from commercial fishing line, that are placed inside a metallic structure with top and bottom plates in which holes were drilled to ensure accurate positioning of the rods. The samples are approximately 100 mm wide and 150 mm tall, and thus much larger than the spot illuminated by the transducers.

Numerical simulations are performed using the ATILA finite element (FE) code.[20] A 2D domain is considered, with a plane wave of chosen frequency normally incident on a PC slab of finite thickness, and infinite width (obtained by means of periodic boundary conditions on the sides). Nylon losses are taken into account by adding an imaginary part to its bulk modulus, equal to 6% of the real part. To avoid including near field effects in the scattering parameters of the slab, transmitted and reflected fields are measured 4 mm away from the slab. At frequencies higher than c/a, with c being the sound velocity in water and a the lattice constant, diffraction orders can appear,[16] i.e. transmitted beams with propagation directions different from the slab normal. In the experiments, they are naturally discarded, since the receiving transducer is located far away from the surface, aligned with the source transducer. In the simulations, they are removed by filtering the fields in water.

The transmission phase used for the determination of the dispersion curves, both in experiments and simulations, is the phase shift between two planes located in water, half a layer away from the center of the surface rods. In other words, the phase shift in water is deduced up to those planes. This definition is well adapted to study PC systems, since the distance between those reference planes is equal to an integer number of individual layer thicknesses. However, it is different from the most natural definition for random systems (which would be the two planes in contact with the farthest nylon rods on opposite faces of the sample). In all cases, real wave vector values are deduced directly from the transmission phase by dividing it by the slab thickness (i.e. the distance between the phase reference planes). For the simulations, other wave vector extraction methods[21,22] can be used, since we also have access to reflection parameters. They give quite similar results, apart from the Bragg gaps where group velocity is slightly higher.

Previous studies[23] have shown that random collections of such rods in water present two hybridization gaps in the frequency range of interest, around 1 and 1.6 MHz for a rod radius of

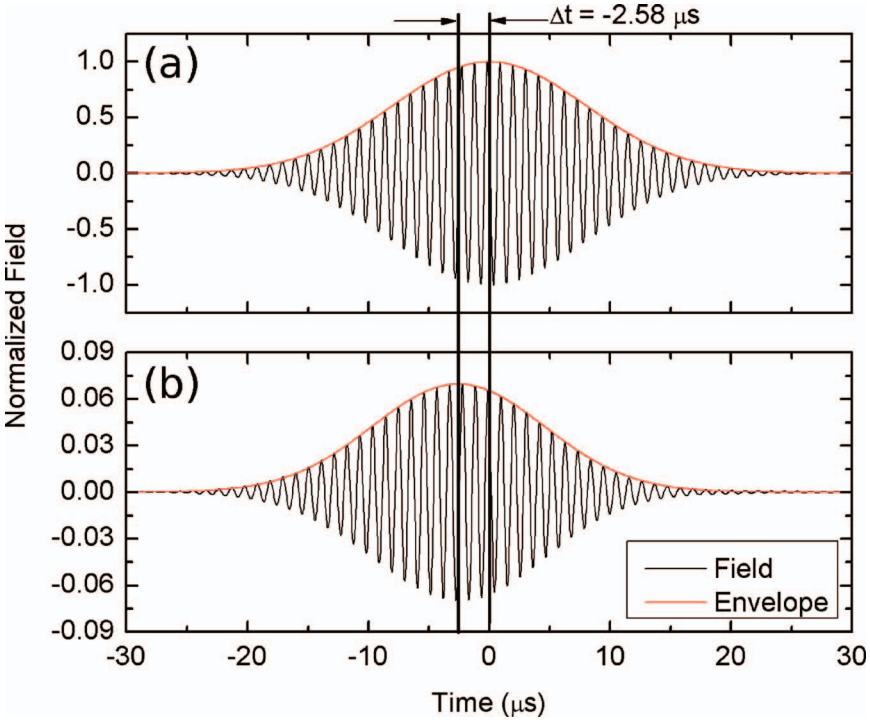

FIG. 3. (Color online) (a) Incident and (b) transmitted time pulses obtained when the experimental pulses are frequency filtered using a digital narrow-bandpass Gaussian filter, for the six-layer thick-PC of nylon rods in water with a filling factor of 40%, at 28°C.

0.23 mm. The first PC considered has a filling factor of about 40% (lattice constant of 0.693 mm). As shown in Fig. 2, it exhibits two gaps, around 1 and 1.5 MHz. They differ greatly, both in terms of wave vector values and dispersion. Inside the first gap, the effective wave vector is largely imaginary, and its real part has a frequency dispersion which corresponds to a negative value of the group velocity. This property is characteristic of resonance related gaps. It should be pointed out that in the presence of strong frequency dispersion and attenuation, the group velocity cannot describe the propagation of energy inside the system[24] although the group velocity does still accurately describe coherent pulse propagation of a sufficiently bandwidth-limited pulse.[25] In fact, such dispersions are better understood in the time domain, where it can be shown that they correspond to a strong pulse reshaping phenomenon which does not violate causality. Figure 3 illustrates the effect, showing the incident and transmitted pulses obtained when the experimental pulses are frequency filtered using a narrow-band Gaussian filter (with a bandwidth of 0.02 MHz for the pulses in Fig. 3). From the measurement of the negative time shift between the peaks of the pulse envelopes, the group velocity can be directly determined. As shown in Fig. 4, the values obtained with this method are consistent with those deduced from the derivative of the experimental dispersion curve. Additionally, they are in good agreement with those deduced from the simulated dispersion curve. Thus measurements of negative group velocity can be used to identify pure hybridization gaps experimentally. Inside the second gap, the effective wave vector is also largely imaginary, since the waves inside the crystal are mostly evanescent. In addition to the complex transmission coefficient, the FE simulations also give access to the local field maps, both in the water matrix and the nylon rods. They show that, in the second gap, field patterns in successive layers of the PC slab are opposite in phase (and rapidly decaying). Thus, this second gap is predominantly Bragg-like, since the transmission phase is a multiple of π. Unlike for the random system, no resonant feature can be spotted around 1.6 MHz. Nevertheless, the existence of the second resonant mode is believed to play a role in the very wide character of this gap.

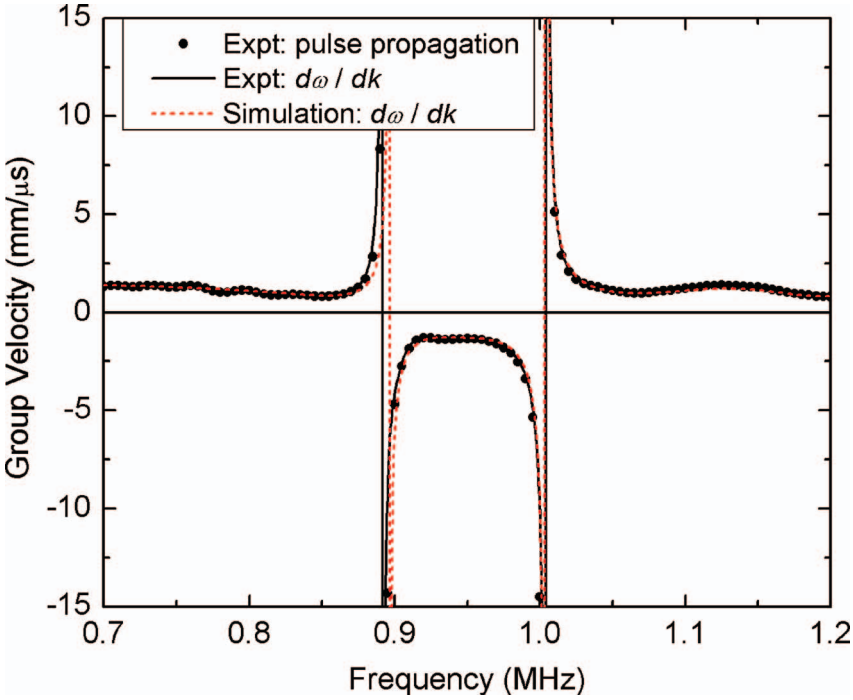

FIG. 4. (Color online) Evolution of the experimental (black) and simulated (red) group velocity as a function of frequency, for the six-layer thick PC of nylon rods in water with a filling factor of 40%, at 28°C. Values are either deduced from the pulse time delays (circles) or calculated from the slope of the dispersion relations (solid and dashed lines, respectively for experiments and simulations).

IV. MODIFIED PC WITH OVERLAPPING HYBRIDIZATION AND BRAGG GAPS

Let us now modify the PC in order to overlap the hybridization and Bragg gaps. This can be easily achieved by choosing a different lattice constant, which greatly shifts the Bragg gap frequencies while keeping the hybridization gap frequency almost constant. With a lattice constant of 0.98 mm (filling factor of about 20%), the Bragg gap should be shifted down to about 1 MHz. Additionally, a finer tuning of the system can be achieved by influencing the shear velocity of the nylon rods, which leads to shifting their resonance frequency. As previously mentioned, different experimental conditions have a significant effect on shear velocity of nylon. Here, we will use temperature variation as our tuning tool. It should be noted that water acoustic parameters are also dependent on the temperature. However it can be shown numerically that this additional parameter variation has almost no effect on the general behavior of the system, as the changes for water are quite small.

Figures 5 and 6 show, respectively, the experimental and simulation results at three different temperatures for a six-layer thick sample. In the simulations, the shear velocity is the only fitting parameter. For the three temperatures 17, 26.5 and 29.4°C, the best fits are obtained with shear velocity values of 1000, 940 and 860 m/s, respectively. This variation is consistent with published studies on the properties of polymers.[26]

In all cases, the crossing of the boundary of the first Brillouin zone (around 865 kHz) shows no sign of the opening of a Bragg gap. It is replaced by a branch with strong attenuation, where the group velocity initially decreases rapidly, immediately followed by a connection to a vertical part. The frequency range of this branch corresponds to the one expected for the combination of Bragg and hybridization effects. Beyond, the next passband opens up. Around 1.6 MHz, as in random collections of rods, a smaller transmission dip related to another resonant mode can be spotted.

It can be seen that nylon shear velocity variations have a strong influence on both the frequency and the level of the transmission dips. Interestingly, they also appear to impact the behavior at

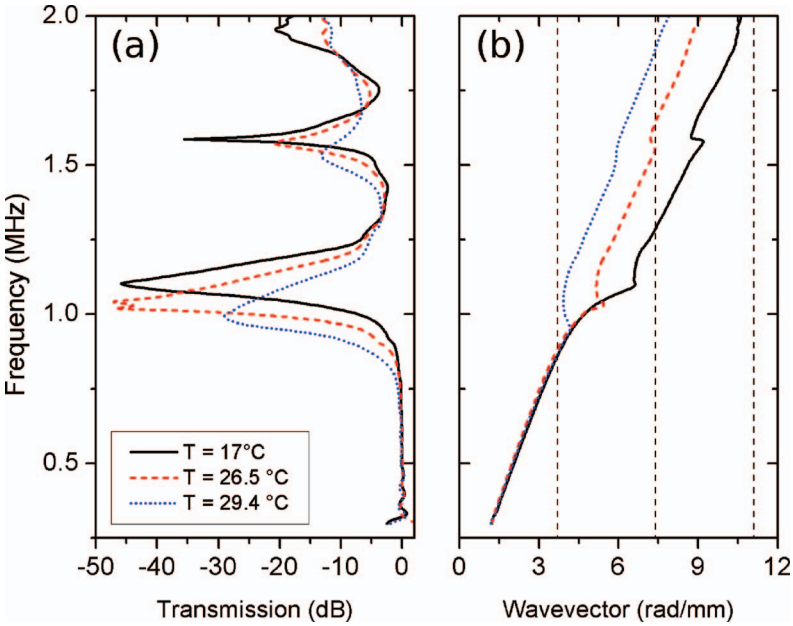

FIG. 5. (Color online) Experimental (a) transmission coefficient and (b) wave vector as a function of frequency, obtained for the six-layer thick PC of nylon rods in water with a filling factor of 20%, at three different temperatures: 17 (black solid line), 26.5 (red dashed line) and 29.4°C (blue dotted line). The vertical dashed lines show the position of the limits of the first three Brillouin zones.

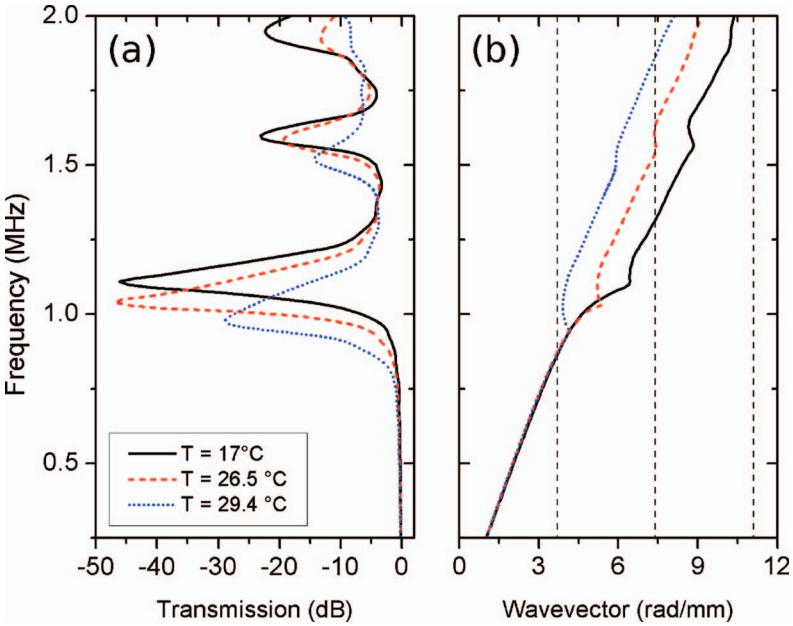

FIG. 6. (Color online) Simulated (a) transmission coefficient and (b) wave vector as a function of frequency, obtained for the six-layer thick PC of nylon rods in water with a filling factor of 20%, at three different temperatures: 17 (black solid line), 26.5 (red dashed line) and 29.4°C (blue dotted line). The vertical dashed lines show the position of the limits of the first three Brillouin zones.

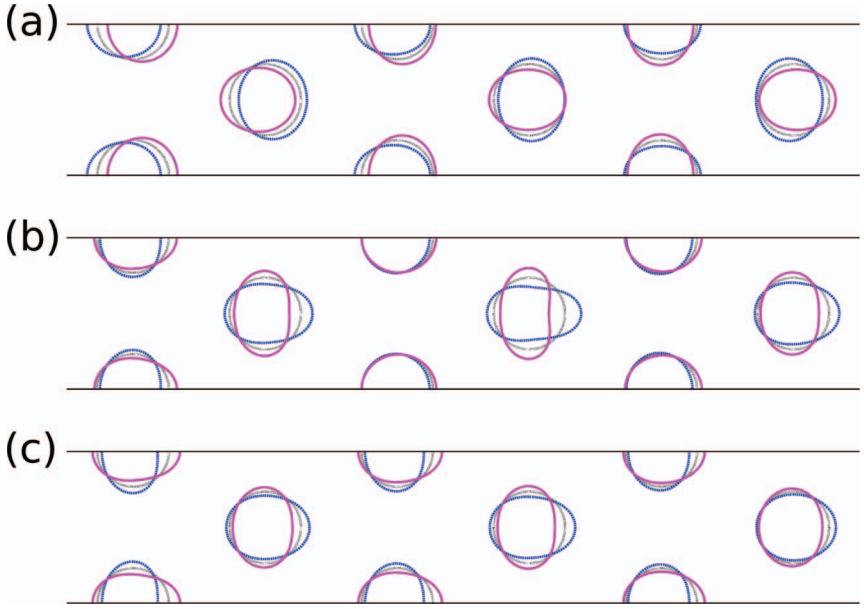

FIG. 7. (Color online) Simulated normalized displacement field map at (a) 800, (b) 1110 and (c) 1130 kHz for the six-layer-thick PC of nylon rods in water with a filling factor of 20% and a temperature of 17°C, with a propagation direction to the right. The two horizontal black lines represent the side boundaries of the domain, which are periodic. The curved lines show the boundaries of the rods (with the normalization of displacements described in the text) at two phase values in quadrature (magenta and blue curves) and at rest (circular dotted black curves).

higher frequencies by introducing "shifts" in the dispersion curves. However, in the transmission band around 1.3 MHz, those shifts correspond to the addition of multiples of 2π radians in the transmission phase, and cannot be related to fundamentally different behavior. In other words, at the hybridization gap, the interaction between the resonances of the rods and the destructive interferences of the waves scattered by the same rods gives rise to a frequency region where the dispersion branch can connect differently to the higher transmission band, depending on the exact frequency of the resonance with respect to the Bragg gap.

In the dispersion curves shown here, we consider that the wave vector as a function of frequency (and its frequency derivative) should be continuous. On the other hand, we could also consider that, since the behavior is the same in all cases around 1.3 MHz (in terms of transmission values and field maps), the wave vector should be the same at that frequency, and introduce a discontinuity at the hybridization gap. Both points of view correspond to an "atypical" dispersion and lead to questioning the physical meaning of the wave vector values inside this combined Bragg-hybridization gap.

Additional insight into the origin of the atypical dispersion characteristics can be gained considering the simulated displacement field maps. Figure 7 shows the normalized displacement of the boundaries of the scatterers for the simulation with a 17°C temperature, at three different frequencies. In the figure, normalization is chosen in order to cancel the vanishing nature of the signal propagating inside the crystal (i.e. displacement vectors are multiplied by a factor $e^{k''y}$, with k'' the imaginary wave vector and y the position along the propagation direction).

The first frequency shown in Fig. 7, 800 kHz, is located in a range where the frequency dependence of the wave vector is still linear. Even though the displacement map shows some deformation of the rods from a circular to oval cross section (which may be referred to as "ovalization"), a significant displacement of the whole rod can also be observed. The second frequency, 1110 kHz, corresponds to the maximum of the attenuation. The fact that the displacement field is dominated by the quadrupole resonance is particularly visible in the second, fourth and sixth layers. Also, the phase appears to be similar in those three layers, which would indicate that the phase shift between points separated by two layers is close to 2π. This suggests that the behavior is influenced by Bragg scattering, which would impose a phase shift between two successive layers equal to a multiple of π. However, if successive layers are considered, the phase relationship is much less visible. By

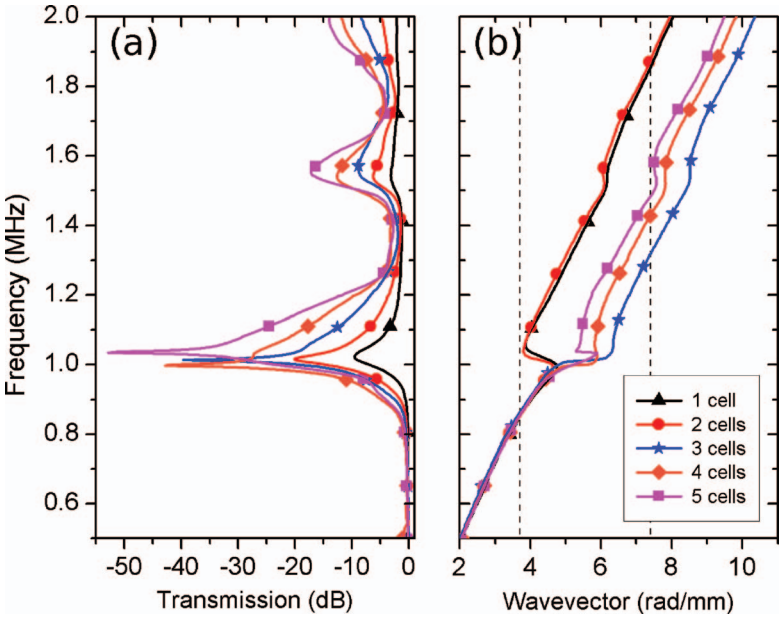

FIG. 8. (Color online) Experimental (a) transmission coefficient and (b) wave vector as a function of frequency, obtained for five nylon-water PCs of different thicknesses, from one to five layers (lines with black triangles, red circles, blue stars, orange diamonds and magenta squares, respectively), with a filling factor of 20%.

contrast, interpretation of the fields at 1130 kHz (third case) is straightforward. At that frequency, the quadrupole resonance is clearly visible, as well as the phase opposition between successive layers. This last characteristic indicates that the pass band which starts just above 1130 kHz should begin at the M point (and not the Γ point, since in that case successive layers would be in phase).

The difference in behavior between 1110 and 1130 kHz strengthens the idea that dispersion is atypical in a very limited frequency range. At 1110 kHz, the total phase shift though the PC slab cannot be used directly to determine the local phase evolution between layers, unlike at 1130 kHz.

Additional insight into this phenomenon can be acquired by studying crystal slabs of different thicknesses. Figure 8 shows experimental results obtained for 1- to 6-layer slabs, at the same temperature. Interestingly, they show that the "shifts" in the dispersion curves also depend on the number of layers. Again, the dispersion branches at the hybridization gap connect to higher branches which only differ by an integer number of 2π phase shifts in the transmission phase. This translates into $2\pi/nd$ shifts for wave vector values, with n the number of layers and d the layer separation, which explains why the different dispersion branches shown in the figures are not regularly spaced (unlike for the temperature study). Also, depending on the slope of the connection to the higher branch, the shifting phenomenon affects the transmission level close to the resonance, which is therefore no longer a linear function (in dB) of the number of cells.

Simulation results, shown on Fig. 9, are again remarkably close to the experiments even though, close to the resonance frequency, some differences can be spotted between the shapes of the transmission dips.

These observations confirm that, due to the combination of resonant and Bragg effects, the extracted wave vector loses its usual meaning inside the lower part of the gap: the wave vector extracted on a crystal of a given thickness cannot be used to predict the transmission phase for another crystal thickness. In a narrow frequency band around 1 MHz, transmission phase is a result of the coupling of the rods resonant states inside the crystal. The characteristics of the coupling can be affected by the position of the resonant frequency with respect to the Bragg gap, or by changing the number of coupled resonators (number of rows). Above this narrow band, the behavior of a usual phononic crystal structure is restored.

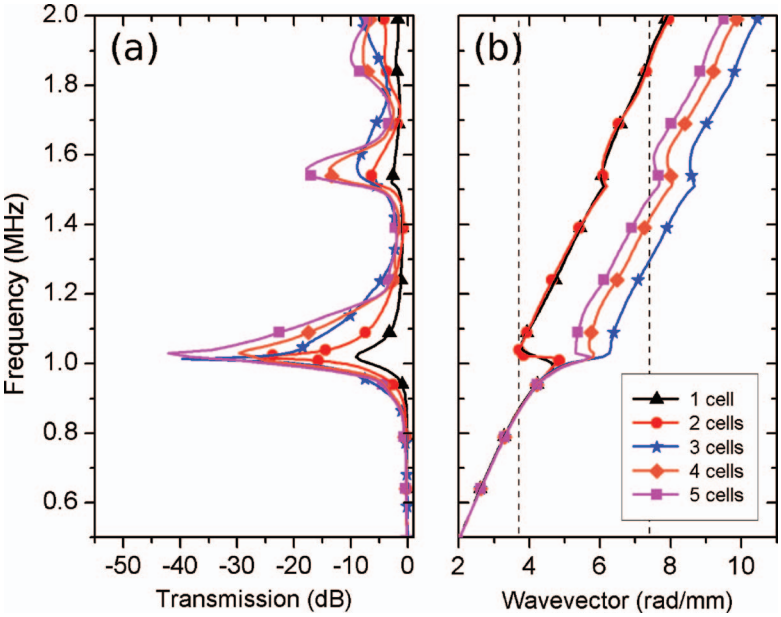

FIG. 9. (Color online) Simulated (a) transmission coefficient and (b) wave vector as a function of frequency, obtained for five nylon-water PCs of different thicknesses, from one to five layers (lines with black triangles, red circles, blue stars, orange diamonds and magenta squares, respectively), with a filling factor of 20%.

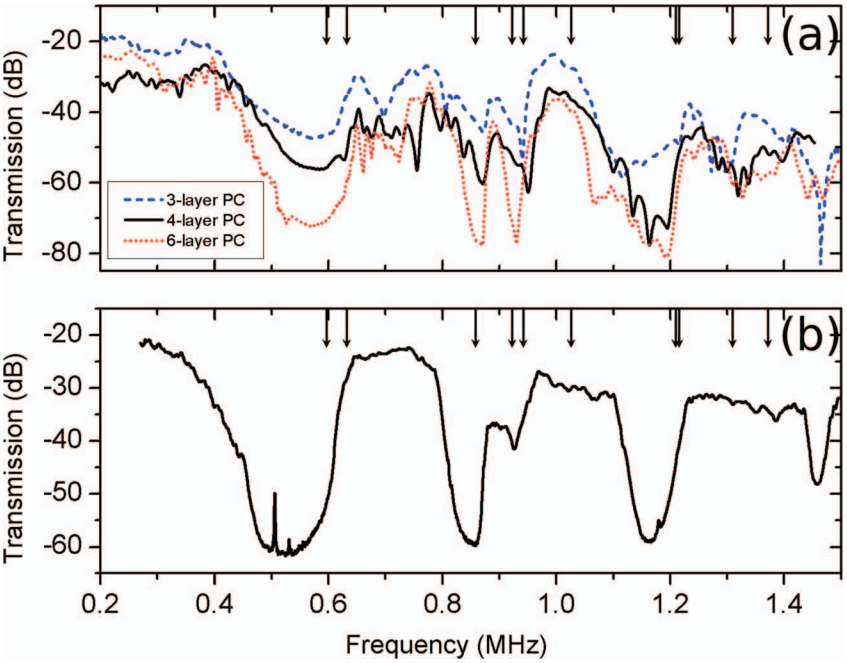

FIG. 10. (Color online) Experimental transmission spectra obtained for (a) three, four and six layers of the opal-like PC structure of weakly sintered aluminum beads (dashed blue line, solid black line and dotted red line, respectively), and for (b) a disordered sample made from the same type of sintered beads. The arrows indicate the frequencies of the resonant modes of the individual beads.

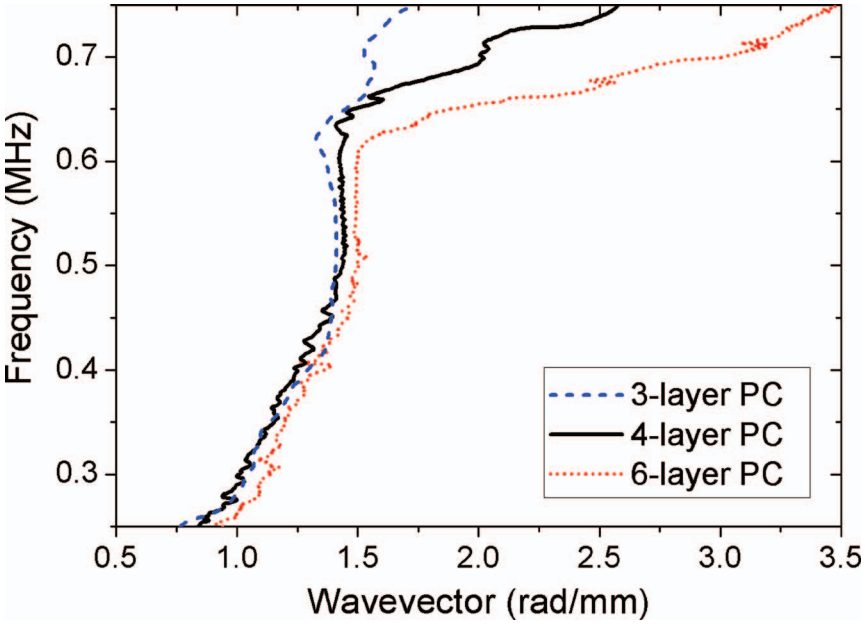

FIG. 11. Experimental dispersion relation (frequency versus wave vector), obtained for three, four and six layers of the opal-like structure of weakly sintered aluminum beads (dashed blue line, solid black line and dotted red line, respectively)

V. BAND GAPS IN SINGLE-COMPONENT OPAL-LIKE PC

A third mechanism leading to the formation of band gaps occurs in 3D phononic crystals with a similar structure to naturally occurring opals. Such crystals are made from a single component, so that there is no embedding medium surrounding scattering inclusions. While some experiments have been performed on SiO_2 opal films with small particle sizes commensurate with optical photonic properties, the high phonon frequencies involved in such small structures make experimental studies of the phononic crystal properties challenging.[27] We investigate an opal-like 3D phononic crystal made by weakly sintering aluminum beads to form a solid network structure. This mesoscopic opal has some advantages for a detailed investigation of its properties since the size of the beads can be chosen to enable measurements in the ultrasonic frequency range. Figure 10(a) shows the experimental transmission spectrum obtained for three crystals, with three, four and six layers, made from face-centered cubic arrays of 4.11-mm-diameter aluminum beads stacked along the [111] direction and then sintered at 630°C. The transmission coefficient exhibits several passbands and gaps above the low frequency effective medium regime. They are related to the presence or the absence of coupled resonant modes of the beads due to necks that are formed between the beads during sintering. The crystals investigated here are deliberately weakly sintered, so that the necks are narrow and the spherical bead shape is preserved. Interestingly, as shown in Fig. 10(b), gaps persist when the periodic arrangement is lost, i.e., when a "mesoglass" of randomly-positioned sintered aluminum beads is considered.[28,29] This indicates that no Bragg scattering is required for band gap formation. In fact, the behavior is analogous to the tight binding model for electronic systems, with the resonant frequencies corresponding to energy levels of atoms. Just as the coupling between adjacent atoms causes the electronic energy levels to broaden into bands, the weak elastic coupling between the beads leads to a band of coupled resonances that form the high frequency pass bands of the structure. The centers of the pass bands are shifted up in frequency relative to the resonance frequencies of the individual beads due to the coupling between them. In-between, gaps can be observed provided that the coupling is not too strong. Consequently, the transmission spectrum can be analyzed as a low frequency pass band (up to approximately 400 kHz, which would be the cutoff frequency for a phononic crystal of point-like scatterers with no internal modes), followed by alternating band gaps and pass bands related to the coupled resonant modes.

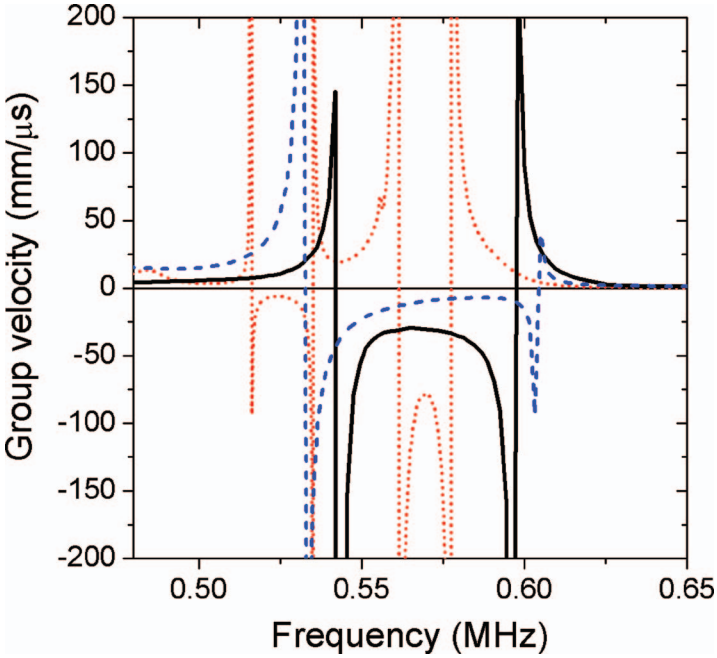

FIG. 12. Experimental group velocity as a function of frequency, obtained for three, four and six layers of the opal-like structure of weakly sintered aluminum beads (dashed blue line, solid black line and dotted red line, respectively).

The measured dispersion relations in the vicinity of the lowest frequency band gap are shown in Fig. 11. The frequency rises abruptly in the gap region, where the wave vector is around 1.4 mm^{-1}, with a negative slope over at least part of the gap in each sample. Thus it is of interest to measure the group velocity directly from pulse transmission experiments, using the same frequency filtering technique described above. The results for the group velocity are shown in Fig. 12. In the middle of the gap, where the transmission coefficient is found to decrease exponentially with thickness, the group velocity becomes more negative as the thickness increases. This behavior is reminiscent of the positive increase in v_g with thickness discussed for pure Bragg gaps in section II, except that here v_g is negative and decreases linearly with thickness. This suggests that the transmission through the band gap of this mesoscopic opal is also dominated by a tunneling mechanism, with the remarkable feature that tunneling in this case appears superluminal.

VI. CONCLUSIONS

We have investigated the different underlying mechanisms that can lead to the formation of bands gaps in mesoscopic phononic structures, both periodic and randomly organized. It was shown that they have distinct characteristic properties, particularly in terms of phase and group velocity, as determined from the transmitted signals. In some cases, tunneling phenomena have been demonstrated. Additional insight into the local origin of the transmission properties can be gained exploiting the simulated field maps inside the structures. Moreover, with appropriately designed structures, we have shown that it is possible to tune the frequency regions where band gaps of different origins develop, so that they can be made to overlap. In the case considered in this paper, hybridization and Bragg gaps were overlapped so that the interaction between these two mechanisms could be investigated. Parametric studies, in which material parameters and sample thickness were varied for both experiments and numerical simulations, show that the dispersion relation between frequency and wave vector is atypical for a phononic crystal. The phenomenon is related to the coupling mechanism between the resonant states of neighboring rods, and will be the subject of further in-depth studies to elucidate this anomalous behavior.

[1] M. S. Kushwaha, P. Halevi, L. Dobrzynski and B. Djafari-Rouhani, Phys. Rev. Lett. **71**, 2022–2025 (1993).
[2] Z. Liu, X. Zhang, Y. Mao, Y. Y. Zhu, Z. Yang, C. T. Chan and P. Sheng, Science **289**, 1734–1736, (2000).
[3] S. Yang, J. H. Page, Z. Liu, M. L. Cowan, C. T. Chan and P. Sheng, Phys. Rev. Lett. **88**, 104301 (2002).
[4] J. H. Page, S. Yang, Z. Liu, M. L. Cowan, C. T. Chan and P. Sheng, Z. Kristallogr. **220**, 859–870 (2005).
[5] J. Liu, L. Ye, D. A. Weitz and P. Sheng, Phys. Rev. Lett. **65**, 2602–2605 (1990).
[6] X. Jing, P. Sheng and M. Zhou, Phys. Rev. Lett. **66**, 1240–1243 (1991).
[7] M. L. Cowan, J. H. Page, and Ping Sheng, Phys. Rev. B **84**, 094305 (2011)
[8] M. Sigalas, M. S. Kushwaha, E. N. Economou, M. Kafesaki, I. E. Psarobas and W. Steurer, Z. Kristallogr. **220**, 765–809 (2005).
[9] J. Li and C. T. Chan, Phys. Rev. E **70**, 055602 (2004).
[10] J. Mei, Z. Liu, W. Wen and P. Sheng, Phys. Rev. Lett. **96**, 024301 (2006).
[11] T. Still, W. Cheng, M. Retsch, R. Sainidou, J. Wang, U. Jonas, N. Stefanou and G. Fytas, Phys. Rev. Lett. **100**, 194301 (2008).
[12] R. Sainidou, N. Stefanou and A. Modinos, Phys. Rev. B **66**, 212301 (2002).
[13] H. Zhao, Y. Liu, G. Wang, J. Wen, D. Yu, X. Han and X. Wen, Phys. Rev. B **72**, 012301 (2005).
[14] V. Leroy, A. Bretagne, M. Fink, H. Willaime, P. Tabeling and A. Tourin, Appl. Phys. Lett. **95**, 171904 (2009).
[15] Suxia Yang, J. H. Page, Zhengyou Liu, M. L. Cowan, C. T. Chan and Ping Sheng, Phys. Rev. Lett. **93**, 024301 (2004).
[16] A. Sukhovich, L. Jing and J. H. Page, Phys. Rev. B **77**, 014301 (2008).
[17] A. Sukhovich, B. Merheb, K. Muralidharan, J. O. Vasseur, Y. Pennec, P. A. Deymier and J. H. Page, Phys. Rev. Lett., **102**, 154301 (2009).
[18] J.-F. Robillard, J. Bucay, P. A. Deymier, A. Shelke, K. Muralidharan, B. Merheb, J. O. Vasseur, A. Sukhovich and J. H. Page, Phys. Rev. B **83**, 224301 (2011).
[19] Z. Liu, C. T. Chan, P. Sheng, A. L. Goertzen and J. H. Page, Phys. Rev. B **62**, 2446–2457 (2000).
[20] *ATILA Finite Element Code for Piezoelectric and Magnetostrictive Transducers Modeling*, User's Manual, Version 5.2.1, ISEN, Acoustics Laboratory, Lille, France, 2002.
[21] V. Fokin, M. Ambati, C. Sun and X. Zhang, Phys. Rev. B **76**, 144302 (2007).
[22] C. Croënne, A.-C. Hladky-Hennion, J. Vasseur and B. Dubus, *Proc. IEEE IUS 2010*, 1861–1864 (2010).
[23] E. J. S. Lee and J. H. Page, *Proc. 30th Symposium on Ultrasonics Electronics*, Kyoto, Japan, 461–462 (2009).
[24] L. Brillouin, *Wave propagation and group velocity* (Academic Press, New York, 1960).
[25] J. H. Page, Ping Sheng, H. P. Schriemer, I. Jones, Xiaodun Jing and D. A. Weitz, Science, **271**, 634-7 (1996).
[26] J. R. Asay, D. L. Lamberson and A. H. Guenther, J. Appl. Phys. **40**, 1768–1783 (1969).
[27] A. V. Akimov *et al.*, Phys. Rev. Lett. **101**, 33902 (2008).
[28] J. A. Turner, M. E. Chambers and R. L. Weaver, Acustica **84**, 628–631 (1998).
[29] H. Hu, A. Strybulevych, J. H. Page, S. E. Skipetrov and B. A. van Tiggelen, Nat. Phys. **4**, 945–948 (2008).